



Article

Evaluation and Structural Optimisation of 0.6 m Impulse Turbine in Dolphin Wave Energy Conversion Device Through Computational Fluid Dynamics and Generative Design

Szymon Szatkowski ¹, Daniel Gonzalez Delgado ¹ , Pablo Jaen-Sola ^{1,*}  and Erkan Oterkus ²

¹ School of Computing, Engineering and the Built Environment, Edinburgh Napier University, 10 Colinton Road, Edinburgh EH10 5DT, UK; szymon.szatkowski@napier.ac.uk (S.S.); d.gonzalezdelgado@napier.ac.uk (D.G.D.)

² Naval Architecture, Ocean and Marine Engineering Department, University of Strathclyde, 100 Montrose St, Glasgow G4 0LZ, UK; erkan.oterkus@strath.ac.uk

* Correspondence: p.sola@napier.ac.uk

Abstract: In this paper, the performance of an adapted design of a 0.6 m impulse turbine in a new wave energy conversion device—the Dolphin device—is evaluated. This study is focused on developing an optimised structure in order to maximise the potential of the device and provide a lightweight and robust novel design. For this purpose, initial studies on the system involved 2D CFD simulations combined with parametric optimisation, which validated the use of the turbine system with water as the working fluid. The obtained component geometries were then used for the creation of a 3D CFD model, which was tested in a set-up dynamic simulation environment. Subsequently, the performance of the system was evaluated through the use of referenced experimental analyses. By taking into account the loading conditions present at the blades, as well as the inherent typical loads caused by the rotational speed of the turbine, the system was then optimised using generative design processes. Through the applied methodology, the performance of the turbine was predicted to be 61.79%. Moreover, the generative design optimisation showed a reduction in mass of 60.226% for the blade structure and 69.523% for the rotor structure.

Keywords: wave energy; computational fluid dynamics; dynamic mesh; impulse turbine; load mapping; generative design



Citation: Szatkowski, S.; Gonzalez Delgado, D.; Jaen-Sola, P.; Oterkus, E. Evaluation and Structural Optimisation of 0.6 m Impulse Turbine in Dolphin Wave Energy Conversion Device Through Computational Fluid Dynamics and Generative Design. *J. Mar. Sci. Eng.* **2024**, *12*, 2259. <https://doi.org/10.3390/jmse12122259>

Academic Editor: Barbara Zanuttigh

Received: 18 October 2024

Revised: 21 November 2024

Accepted: 28 November 2024

Published: 9 December 2024



Copyright: © 2024 by the authors. Licensee MDPI, Basel, Switzerland. This article is an open access article distributed under the terms and conditions of the Creative Commons Attribution (CC BY) license (<https://creativecommons.org/licenses/by/4.0/>).

1. Introduction

1.1. Project Background

The following investigation of the turbine system presents a study on a 0.6 m flooded impulse turbine in a wave energy conversion device, also called the Dolphin device. The development of the Dolphin device encompasses various areas of studies related to engineering such as complex dynamic computational fluid dynamics simulations, design for manufacturing and parametric optimisation. It is a novel approach towards the challenging idea of capturing the elusive wave energy. The aim of the Dolphin device is to unlock that potential and contribute towards the goal of sustainable, diverse, and green energy sources.

The overall schematic of the Dolphin device can be seen in Figure 1. It is composed of four major component groups, which were colour-coded:

- Red—control components (valves);
- Blue—turbine assembly;
- Green—float and pumping chamber assembly;
- Grey—connection pipes.

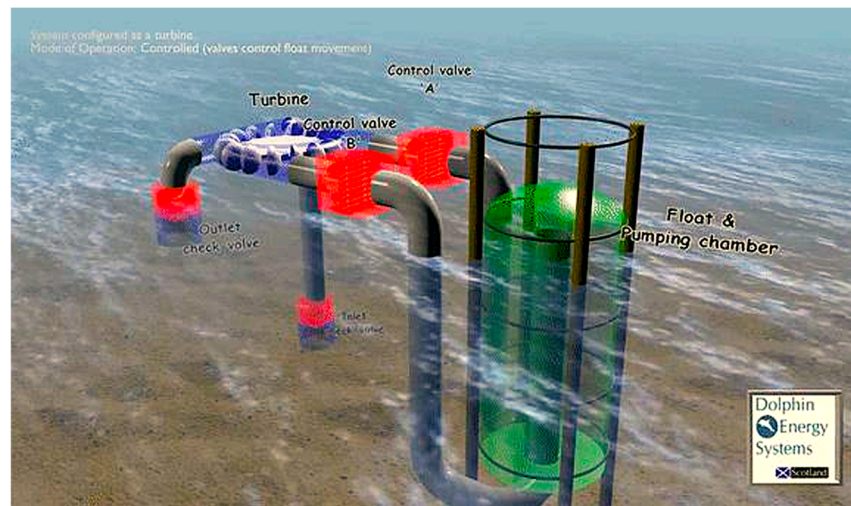


Figure 1. Dolphin wave energy converter schematic overview [1].

Throughout the operational cycle, the float follows the movement of the sea waves. On the upward movement of the sea waves, the float begins its upstroke. On the downward movement of the sea waves, the float follows with a downstroke. This is the initial stage by which the energy is captured by the device. The float is also directly mounted on top of a pumping chamber, which causes the pumping chamber to have a varying and changing volume. Because of this relation, the system is able to transport the working fluid taken from the water body via negative pressure, in this case, the sea water, throughout the system (Figure 2).

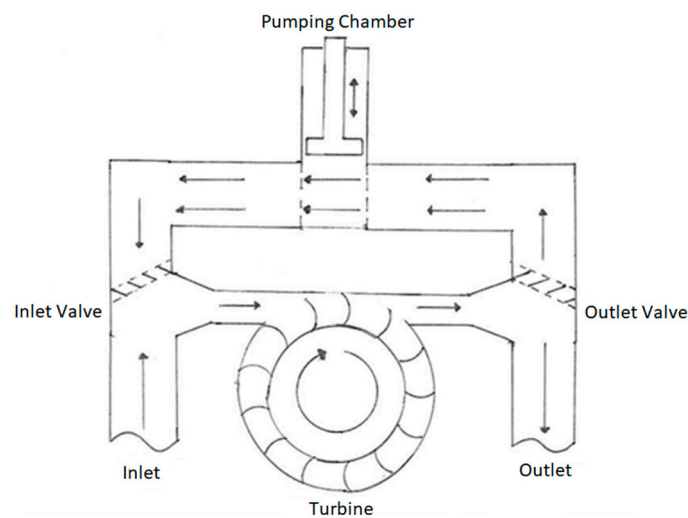


Figure 2. Schematic of the dolphin wave energy converter.

The valves ensure that the direction of travel, as well as the extent of it, is accurately controlled. The inlet and outlet valves control the flow direction, whereas control valves (also called shutter valves) A and B restrict the flow throughout the system. The shutter valves A and B work in an alternating manner, in synchronism with the upward and downward movement of sea waves. This means that on the upstroke of the float, shutter valve A located directly before the pumping chamber remains open, whereas shutter valve B located directly after the pumping chamber remains closed (Figure 3). On the downstroke of the float, shutter valve B is opened, while shutter valve A is closed, allowing for the fluid to flow further down the system.

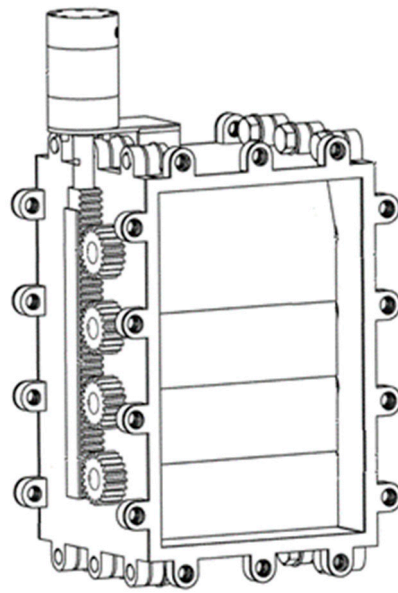


Figure 3. Schematic of shutter valve in closed position [1].

The working fluid then enters the turbine assembly area, where it impacts the turbine blades, transferring its kinetic energy. This promotes the rotational movement of the turbine. The rotational movement is then transmitted to the generator via the gearbox system, and finally, the electrical energy can be produced. The working fluid is then discharged from the system, back to the water body environment. Then, the operational cycle can start anew.

The performance of the Dolphin device is closely related to the environmental conditions, as well as the operational capabilities of the designed components. Therefore, it is necessary to carry out accurate and trustworthy studies aimed at the improvement of the system via computational simulations. The results of the conducted investigations carry a significant importance, as they will allow the designers to identify and correct potential problems. Such an approach will significantly contribute towards the overall improvement of the Dolphin device.

1.2. Wave Energy Devices Overview

Wave energy conversion devices come in various designs and configurations, each tailored to optimise energy extraction from different types of wave motion and environments. A number of wave energy conversion devices were investigated by academia and industry. When designing a wave energy converter, it is essential to familiarise oneself with these existing solutions to understand their strengths, limitations, and suitability for various locations and wave conditions. They mainly differentiate into three categories: onshore, nearshore, and offshore devices. Below, you can find examples for each of the categories with a brief overview.

- **Oscillating Water Column**

The Oscillating Water Column is one of the most established technologies for harnessing wave energy, particularly in onshore applications. They consist of a partially submerged structure with an open bottom that allows water to enter and form an air column. As waves cause the water level inside the chamber to rise and fall, the air above the water is alternately compressed and decompressed, driving a bidirectional air turbine, typically a Wells or impulse turbine, to generate electricity [2]. Notable examples include the LIMPET (Land Installed Marine Power Energy Transmitter) system in Islay, Scotland, and the Pico Power Plant in the Azores, Portugal. An example of such a system was presented in Figure 4. These devices benefit from simpler maintenance and grid connection due to their fixed coastal location, though their performance is somewhat limited by wave energy availability at the shore.



Figure 4. LIMPET power plant, Scotland, reproduced from [3], under CC BY-NC-SA 1.0 licence.

- The Oyster

The Oyster wave energy converter is a nearshore device designed to operate in relatively shallow waters, typically at depths of 10–15 m. Developed by Aquamarine Power, the Oyster is a bottom-mounted, oscillating wave surge converter. It consists of a large, hinged flap that faces incoming waves and sways back and forth with wave motion. This motion drives hydraulic pistons, which pump high-pressure water to an onshore hydro-electric generator [4]. The Oyster's nearshore location provides it with access to energetic wave environments while remaining close enough to shore for easy maintenance and grid integration. Its simple, robust design minimises moving parts in the marine environment, enhancing its reliability and longevity. A schematic of the Oyster is shown in Figure 5.

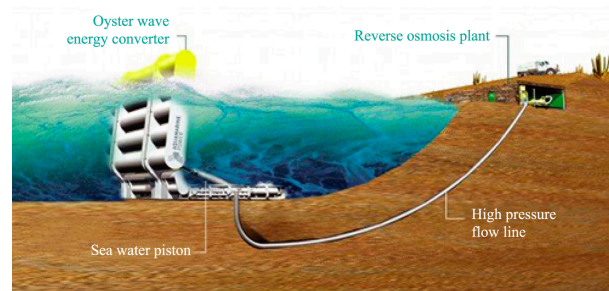


Figure 5. The Oyster schematic [4].

- Wave Dragon

Wave Dragon is an offshore overtopping device designed to harness wave energy in deep-water environments, typically far from the coast where wave energy is more abundant and consistent. Figure 6 presents a schematic of such a system. It uses a large ramp to capture and direct incoming waves into an elevated reservoir, from which water is released to drive multiple low-head hydro turbines, generating electricity. The floating structure is anchored to the seabed and designed to scale up to multi-megawatt capacities. Its offshore location allows it to exploit powerful wave climates, maximising energy output. Additionally, Wave Dragon can act as a breakwater, providing coastal protection [5]. However, its large size and complex anchoring system present challenges in terms of deployment, maintenance, and initial costs.

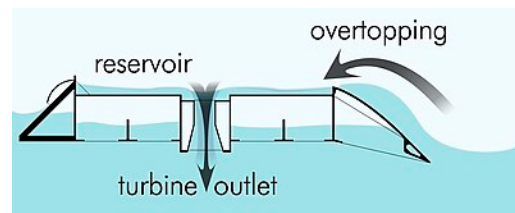


Figure 6. The Wave Dragon schematic [6].

1.3. Significance of Wave Energy Research

In recent years, renewable energy sources have captured the attention of both the media and the public. This is mainly due to the ever-increasing energy prices, the ongoing climate change, air pollution, or simply the vision of decarbonising the economy. Wave energy is a crucial factor in the Net Zero carbon emissions target by 2045 [7]. Scotland's position on the western edge of Europe, combined with its unique geography of seaways and firths, subjects it to intense winds, Atlantic waves, and turbulent tidal currents. This makes the country ideally situated to harness its ocean energy potential, provided the necessary infrastructure and financial support are in place [8,9].

The development of wave energy devices has been very limited when compared to other renewable energy sources. Most of the current real-world applications are focused on research and demonstration, which is represented by the small wave energy capacity of 12.7 MW for total installed devices since 2010 in Europe, as of reports from 2023 [10]. Wave energy converters are widely known for their low maturity in research, high risk, and uncertainty, as well as high initial capital requirements [11]. These factors discourage private investors and enforce the need for public investments to advance research and design activities in the field.

Arguments which promote wave energy were made by a considerable number of researchers. They state that waves possess the highest energy density among renewable energy sources, surpassing wind, solar, biomass, and geothermal [11]. Additionally, according to the US Energy Information Administration, the waves along the United States coasts have the potential to supply 66% of the country's electricity. Moreover, the UK and Ireland were predicted to have a power potential of 27 and 21 GW, respectively, with Ireland and Scotland having higher shares in wave renewable energy. This would represent the potential to meet up to 20–30% of the current electricity demand in the UK and Ireland combined. This makes wave energy a significant potential contributor to enhancing the resilience of the global energy mix [12,13].

Figure 7 illustrates the global wave energy resources, showing that the raw wave power intensity ranges from 50 to 70 kW/m along the coasts of the UK and Ireland. Therefore, the availability of raw wave energy highlights the importance of capturing this elusive energy source, especially when compared to other locations worldwide. With a limited number of conversion devices launched this year, ocean energy is regarded as one of the biggest unexploited sources of renewable energy [3].

The initial slow development of wave energy was further hindered by the lack of demonstrable energy-harnessing capabilities at a low enough cost for commercial use. Sharman [14] asserts that for wave energy devices to become commercially viable, "they need to be cheaper, produce more energy and brave the ocean's brawn better and for longer". Many modern wave energy conversion devices are often outfitted with heavy and expensive hulls that make this technology too expensive to make it viable. "About 35–50% of wave energy costs are spent on structural enhancements" [14]. Similar studies incorporating structural optimisation on wind energy systems showed a significant improvement in efficiency, material costs, and maintenance costs, as well as environmental impact [15]. Although the conducted investigations were applied to machinery of different characteristics and in different working environments, the substantial advantages justify the use of optimisation techniques for wave energy devices. Therefore, it is crucial to conduct studies, which will result in well-optimised and simple but robust and lightweight devices.

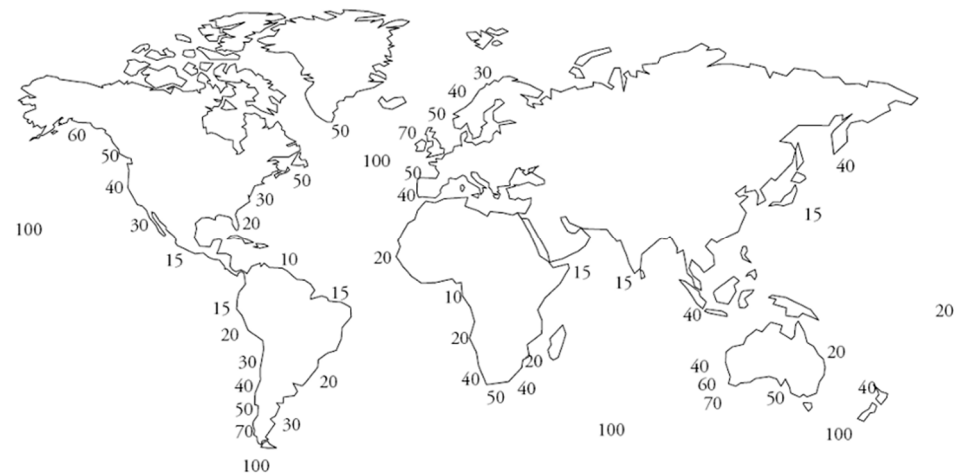


Figure 7. Worldwide wave energy resources (in kW/m) reproduced from [3], under CC BY-NC-SA 1.0 licence.

To facilitate innovation and technological progress, computer-aided engineering has been introduced. This allows academic and industry sectors to identify key parameters of studied objects more quickly and cost-effectively than producing physical prototypes. Advanced simulation software enables an in-depth study of the relationship between designed components and their intended operational environments. A significant feature depicting the efficiency of wave energy conversion devices is computational fluid dynamics (CFD), which creates digital simulations depicting fluid flow and its impact on solid objects [16]. Jeremiah Pastor et al. [17] explore the optimisation potential of point-absorbing wave energy converters (WECs) through numerical modelling. Their approach, utilising ANSYS 2020 software, allows for a detailed examination of buoy geometries and hydrodynamic performance under various sea states. The study demonstrates that conical buoys, with optimised diameter and draft, enhance power absorption efficiency by up to 95% in calm seas. This underscores the significant promise of advanced numerical methods in renewable energy optimisation, offering robust designs tailored for offshore energy platforms. Moreover, Daniel Gonzalez-Delgado et al. [18] show the potential of such investigations on the example of multi-MW offshore direct-drive wind turbine electrical generators through generative design. The mentioned approach allowed for an in-depth analysis of a wide range of unconventional topologies on a tailored, fit-for-purpose strategy. Overall, the referenced study demonstrated over 7% weight reduction and a 40% increase in operational range, which shows the potential of such research [18]. CFD analysis, in combination with structural optimisation processes, gives the researchers a powerful tool to improve the overall performance of the designed components and verify the findings.

This study presents a design analysis of a turbine structure for an offshore wave energy conversion device, integrating computational fluid dynamics (CFD), structural analysis, generative design optimisation, and additive manufacturing principles. A 0.6 m impulse turbine was identified as the optimal solution after initial evaluations. The study involved CFD simulations and parametric optimisation to refine turbine geometry for efficient operation. A 3D model was developed and analysed in Ansys Fluent using a moving mesh for transient simulations. Performance metrics such as torque and power efficiency were calculated. Finally, generative design was applied to reduce turbine assembly mass and enhance manufacturability and sustainability.

2. Methodology

2.1. Methodology Overview

In this study, we present an innovative advanced design analysis of a turbine structure for a new offshore wave conversion device integrating CFD and structural analyses, generative design optimisation, and design for additive manufacturing approaches. Throughout

the conducted investigation, the turbine system of such a device is evaluated and optimised. The preliminary study of the initial concept—a horizontal flooded turbine system—imposed a need for a more appropriate design for the required application. After establishing the favourable characteristics of the system and conducting research on turbine systems, we identified a suitable solution—a 0.6 m impulse turbine—for the purpose of further investigation. Firstly, the working principle of the chosen design was analysed, which allowed for the identification of the required changes in turbine system components, e.g., the elimination of a second set of guide vanes to account for the unidirectional flow of the working fluid. Since the overall fluid behaviour would be altered in the Dolphin device, it was necessary to conduct additional computational fluid dynamic studies on the system. The computational analysis process started with a 2D layout testing of the guide vane and blade set-up. Parametric optimisation was implemented in this process to maximise the potential of the system and tackle the identified problems with water discharge. After obtaining the optimised geometry profiles of the turbine assembly components, the 3D model of the 0.6 m impulse turbine was created. The model was then imported to Ansys 2020 Fluent software for further analysis through 3D CFD transient simulations. In order to proceed with the simulation set-up, the model was meshed, and any necessary boundary conditions were specified. To account for the rotation of the turbine, a moving mesh approach was selected. Subsequently, the flow model and fluid behaviour, as well as the size of the simulation, were specified. Upon completion of the simulations, the performance of the turbine was appraised by using the referenced formulas for torque, power input, and flow coefficients, as well as the efficiency and power generated. After a successful analysis of the turbine, an investigation of the design for manufacture was conducted. A total of 4 design concepts were presented and appraised in relation to the chosen characteristics. The best concept was then selected for further studies involving generative design. For this purpose, the loading of the system was translated and applied to the structure. Lastly, through the use of a generative design process, we were able to present possible geometries which reduce the overall mass of the assembly, and in combination with additive manufacturing, improve the efficiency and sustainability of the structural design techniques. The overall list of objectives, parameters and constraints in this investigation was presented in Table 1. The schematic of the adapted workflow and methodology can be seen in Figure 8.

Table 1. List of design objectives, parameters, and constraints for an impulse turbine investigation.

Design Objectives	<ul style="list-style-type: none"> • Maximise efficiency and power output; • Reduce overall mass; • Enhance durability and structural robustness; • Durability in marine conditions; • Improve water extraction capabilities; • Ensure operational reliability.
Parameters	<ul style="list-style-type: none"> • Blade and guide vane geometry; • Fluid flow characteristics; • Turbine’s rotational speed; • Mesh control parameters; • Loading conditions and model characteristics for generative design.
Constraints	<ul style="list-style-type: none"> • Turbine size; • Turbine tip clearance; • Material choice; • Fluid dynamic constraints; • Manufacturing capabilities; • Computational constraints.

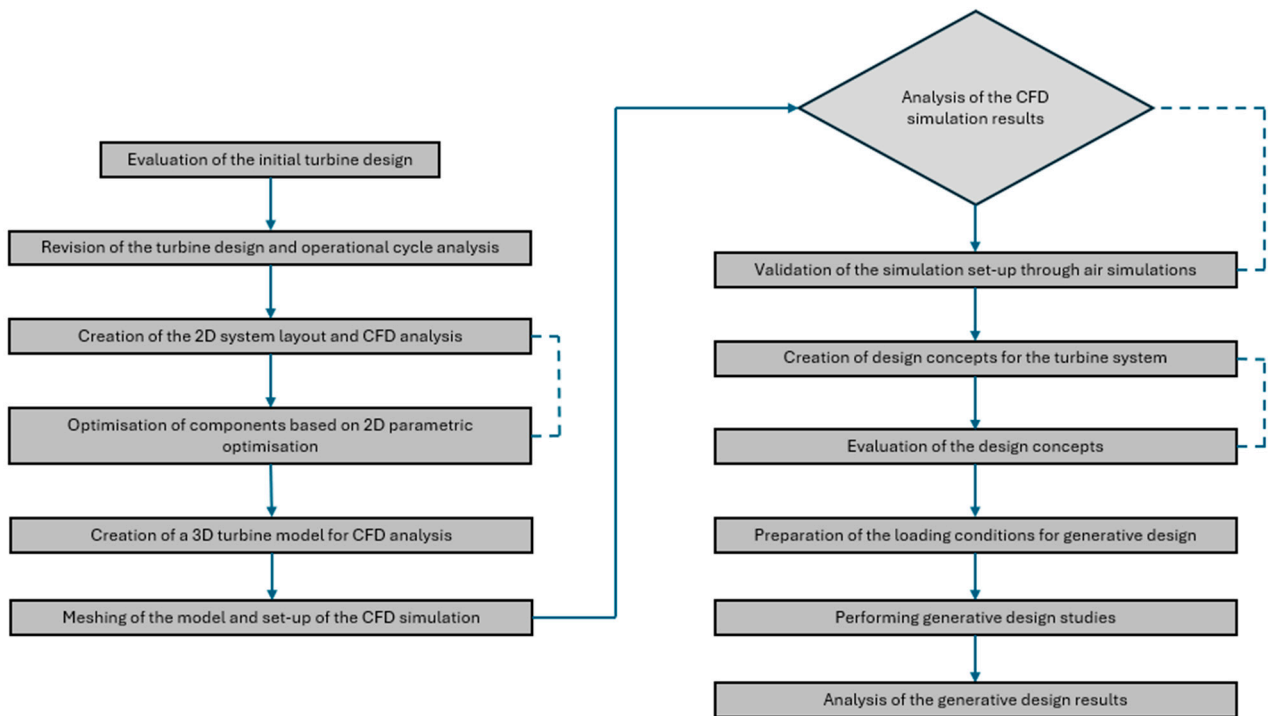


Figure 8. Schematic of the workflow and methodology.

2.2. Initial Turbine Design

Previous studies conducted on the turbine assembly included a design using the horizontal flooded turbine presented in Figure 9.

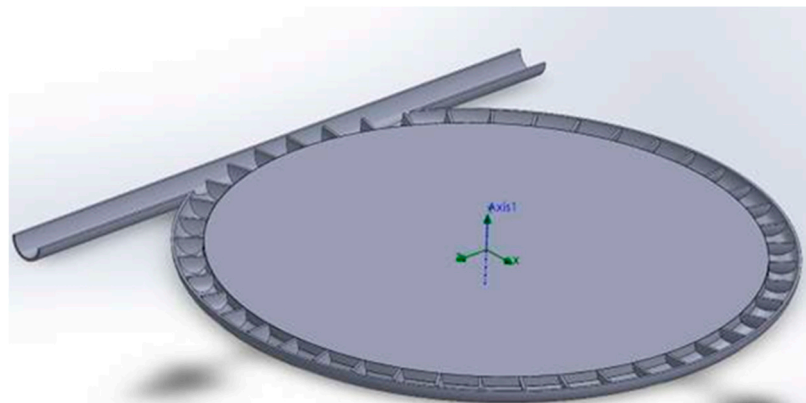


Figure 9. Cross-sectional view of the initial turbine design.

Throughout the investigation, the nozzle and housing pipe diameter were changed with values ranging from 0.03 m to 0.06 m, in order to find the optimal geometries. Moreover, depending on the chosen design of the blades, the rate of rotation was controlled by the ratio between the inlet velocity and turbine blade velocity. Some of the characteristics present in the study were kept constant, such as the flow rate through the system, the outlet pressure, and the ratio of the incoming fluid to the tangential speed of the turbine [19]. By doing this, the author was able to establish consistency across the testing.

During the study, different aspects of the turbine design were evaluated. The main conclusions are as follows:

- The primary performance enhancement is achieved by reducing the cross-sectional area of the pipes.
- The number of blades on the turbine dictates the secondary performance improvement.

- The shape of the blades has minimal impact on the overall performance of the turbine.
- The performance of the turbine is limited by its flooded nature.

The last conclusion was a very alarming finding. The standard usage of a turbine resembling a Pelton wheel does not include the integration of a flooded system. Therefore, the water can be extracted via gravity. The Dolphin device works in hydraulic lock which supports the working principle of drawing and discharging the water through negative pressure. For this purpose, the flooded nature of the turbine is essential. However, upon observation of the fluid behaviour within the turbine housing, it was found that the working fluid would become trapped between the blades during the rotation. This meant that the turbine would not only have to counteract its own weight and other rotational constraints but also exert work on fluid that lost much of its energy on the prior impact on the blades. Ultimately, any improvement in energy extracted by the blades slows the fluid down by a greater degree and will take more energy to evacuate [19].

2.3. Reviewed Turbine Design

Having recognised the issues and limitations that come with the use of the initial design of the horizontal flooded turbine system, we decided to reiterate the design and search for alternative types and geometries. Two main limitations were identified:

- The flooded nature of the turbine, which allows us to maintain a hydraulic lock and negative pressure throughout the system;
- Working fluid velocity loss, which presents a substantial problem when discharging the working fluid from the system and during power generation due to trapped water between the turbine's blades.

Therefore, the new design should allow for improved flow of the working fluid throughout the turbine system. One potential design was identified—an impulse turbine—which presented a very open geometry and potentially improved characteristics. A typical impulse turbine rotor is shown in Figure 10. Figure 11 presents guide vanes that are placed before and after the turbine to allow for the deflection of air onto the turbine's blades. Such rotors are commonly used in OWC wave energy converters. A solution is to use a wave-induced pressure difference to enforce air flow through the turbine [20]. Thus, the proposed turbine would need to be closely studied to validate the change in the working fluid and specify the overall performance.

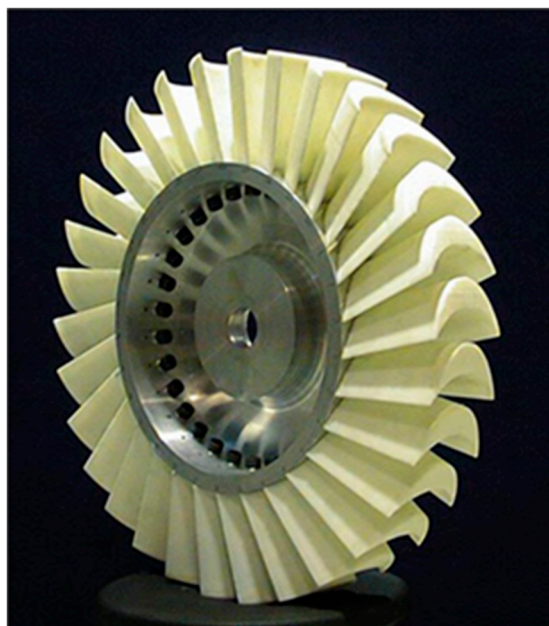


Figure 10. Typical impulse turbine rotor, reproduced from [3], under CC BY-NC-SA 1.0 licence.

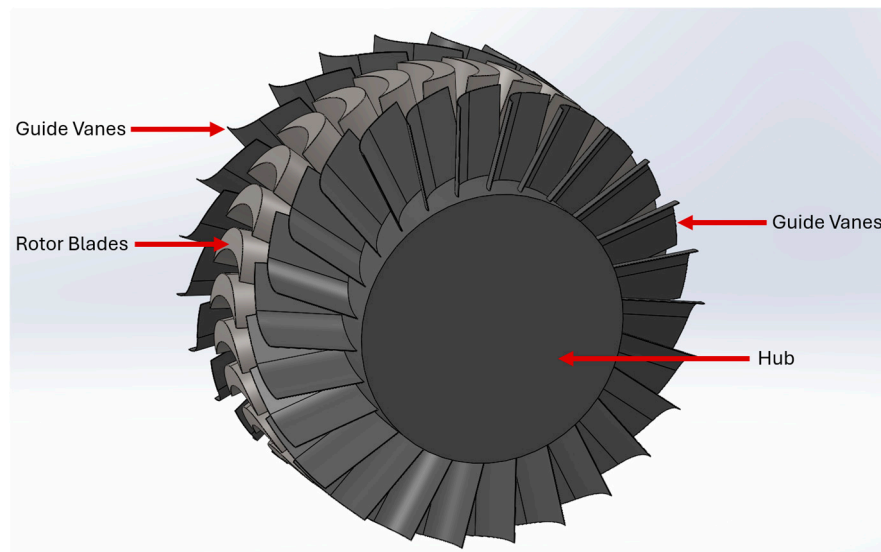


Figure 11. Bidirectional flow impulse turbine.

Firstly, the possible design changes were considered due to the discussed difference in application. The implementation of two guide vane hubs was reduced to one, as the flow of the working fluid would be unidirectional. Moreover, it was recognised that the blade geometry will likely change for the same reason. By referencing previous studies on impulse turbines conducted by Setoguchi et al. [21] and Thakker et al. [22], the turbine size of 0.6 m was chosen to allow for direct referencing of validation processes. The initial blade and guide vane geometry was also implemented as a starting point for future iterations.

2.4. Computational Fluid Dynamics

The computational investigation process started with the creation of a 2D model using a blade and guide vane layout (Figure 12). The layout consists of 2 blades and guide vanes located on a plane. The description of variable dimensions can be seen in Table 2.

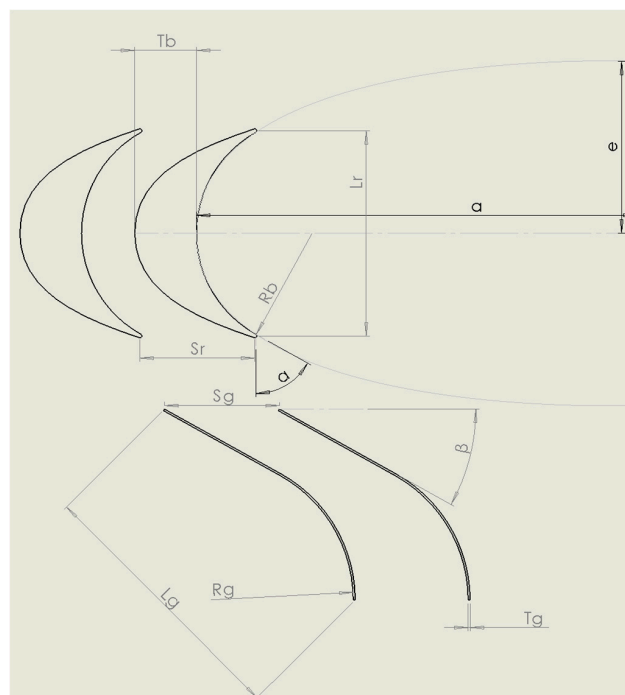


Figure 12. Blade and guide vane layout in 2D model.

Table 2. Two-dimensional layout variable dimensions of blades and guide vanes.

Property	Symbol
Chord Length of the Blade	L_r
Blade Thickness (at Centre)	T_b
Blade Semi-Major Axis	a
Blade Semi-Minor Axis	e
Radius of Circular Arc at the Blade	R_b
Blade Inlet Angle	α
Guide Vane Angle	β
Guide Vane Thickness	T_g
Guide Vane Radius	R_g
Chord Length of the Guide Vane	L_g
Guide Vane Pitch	S_g
Blade Pitch	S_r

Upon completion, the model was imported to Ansys Fluent software for the purpose of computational fluid dynamics investigation. Subsequently, the model was meshed, and mesh quality was evaluated by analysis of orthogonal quality and skewness. The structure and statistics of the exemplary mesh of the initial blade geometry can be seen in Figure 13 and Table 3.

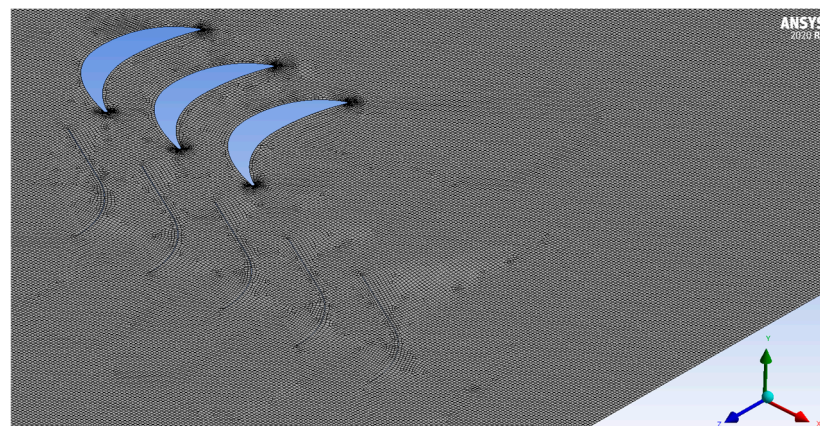


Figure 13. The mesh structure of a 2D planar layout of guide vanes and blades.

Table 3. Mesh statistics and characteristics.

Property	Value
Default Element Size	2 mm
Growth rate	1.2
Maximum Size	2 mm
Curvature Minimum Size	0.02 mm
Curvature Normal Angle	18°
Maximum Skewness	0.637
Minimum Orthogonal Quality	0.64771
Number of Nodes	98,333
Number of Elements	97,209

Initial conditions, such as an inlet velocity of 4 m/s and working fluid properties of water, were applied. The exemplary result of such an investigation in terms of velocity can be seen in Figure 14.

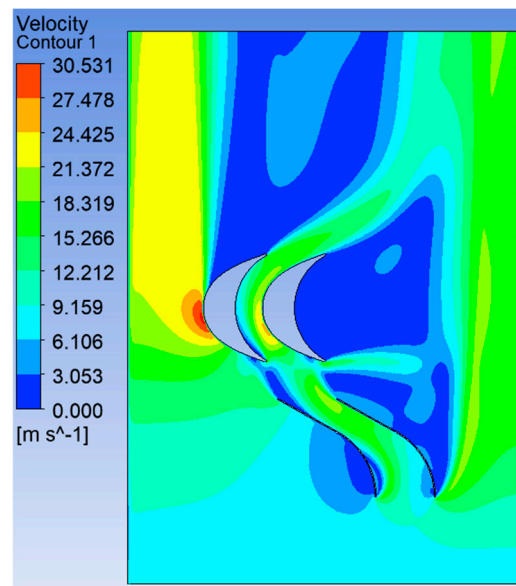


Figure 14. Two-dimensional velocity contours for two-dimensional radius curvature blade.

With the use of additional tools available in Ansys software, namely parametric optimisation, an optimal geometry for the system was found. For this purpose, the system had to be defined with observables—values obtained from simulations that the user intends to change (e.g., lift of the blades, force momentum, etc.), as well as a list of elements requiring change (e.g., profile of the blades or pitch). The schematic showing the areas, which were specified for modification, can be seen in Figure 15.

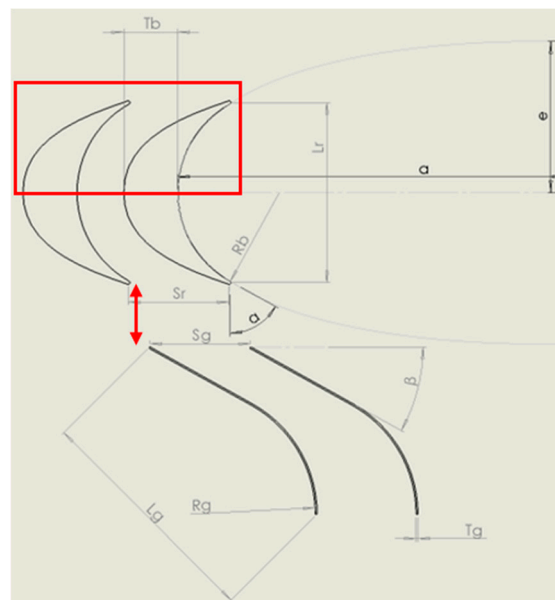


Figure 15. Blade and guide vane layout in 2D model—edited parameters.

Parametric optimisation then attempts to create a specified number of iterations to optimise the system using a specified factor, e.g., an increase in lift of 20%. The result of such a study and the overall geometry of the optimised system can be seen in Figure 16.

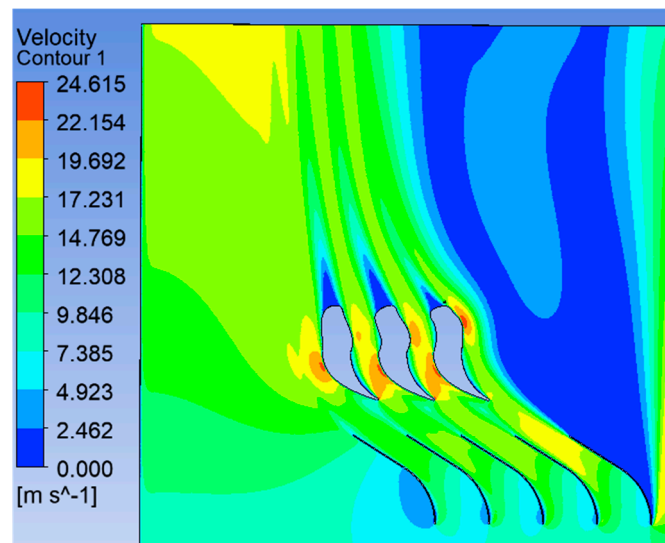


Figure 16. Velocity contour of 2D parametric optimisation generated system.

The water divider was tested separately from the blade and guide vane system layout (Figure 17). The investigation followed a similar approach after specifying the boundary conditions of the system and elements available for optimisation, e.g., the length of the cone and the angle of inclination. The model was optimised in terms of produced drag.

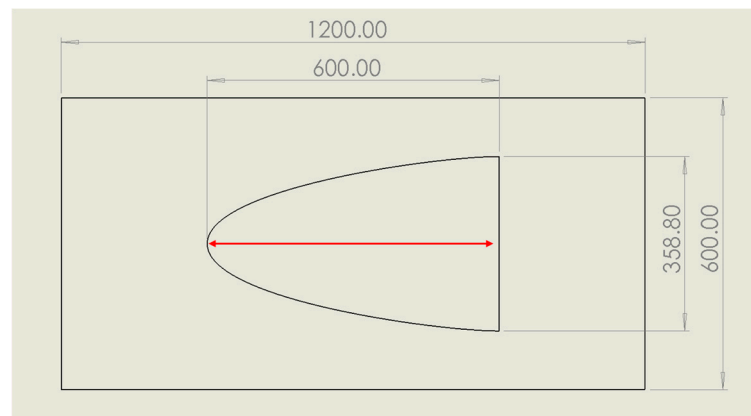


Figure 17. Water divider 2D model.

Over the course of this investigation, an overall improvement in fluid exit velocity can be observed. These preliminary results proved that such a configuration of the turbine system can address the issue of water extraction capabilities. The pitch of the blades, as well as guide vanes, were evaluated and changed accordingly. The resultant change in observable parameters was convergent with the set percentages of improvement. Furthermore, the obtained blade geometry was then simplified for manufacturing purposes, by straightening the second half of the blade profile, which can be seen in Figure 16.

Having validated the use of the impulse turbine with optimised blades and guide vanes, the study proceeded to the next step—the development of a 3D model with the aim of conducting 3D transient CFD simulations. The completed model can be seen in Figure 18. The assembly consists of the following:

- Water Divider—forces the working fluid to flow around the nose of the divider, directly towards the turbine system; prevents loss of momentum from direct impact on the hub.
- Guide Vanes—a total of 28 guide vanes deflect the working fluid onto the blades at 60°.
- Turbine—consists of 30 blades and promotes rotational movement.

- Stationary Domain—a cylinder body encompassing the entire turbine assembly. Essential for specifying the flow domain in Ansys Fluent.
- Rotational Domain—a cylinder body encompassing the turbine; allows us to specify the mesh motion around the rotating component.

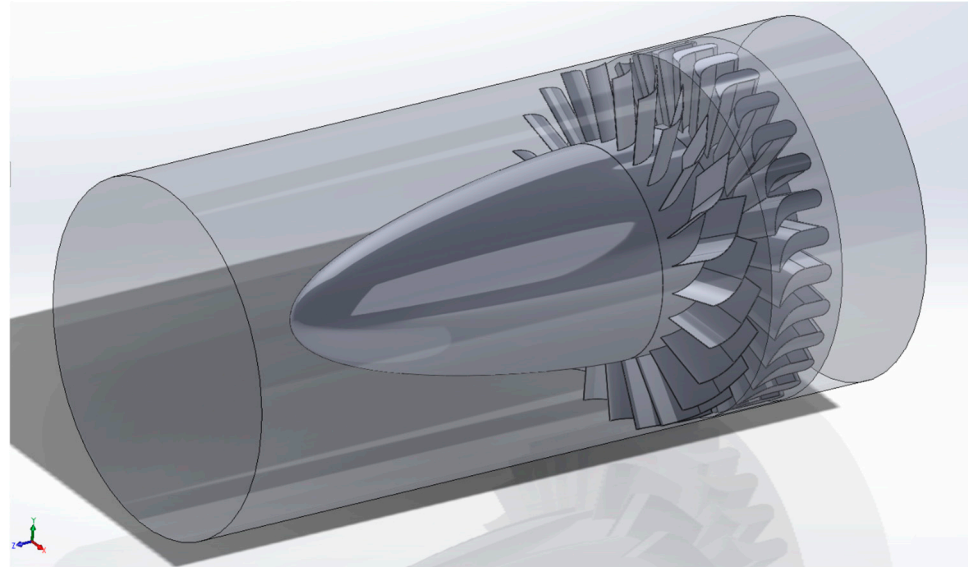


Figure 18. Three-dimensional 0.6 m impulse turbine model for CFD.

The initial revision of the 0.6 m turbine assembly had a total length of 1.3 m. The flow of the fluid in the system was constrained by the stationary domain with an outer diameter of 0.6 m. The tip clearance (distance from the blade’s tip to the outer wall) was set to 1 mm. Such small tip clearance proved to be problematic when meshing the assembly. The issue mainly included unsatisfactory mesh quality, with orthogonal quality being below 0.1 and skewness above 0.9. For the model to compute properly, these conditions needed to be satisfied. The reduction in mesh size would be one of the solutions. Ultimately, the mesh would have to be reduced to such a small size that the simulations with moving mesh would increase the solution times almost by a factor of 2. Therefore, it was decided to increase the tip clearance to 5 mm.

The meshing was achieved by specifying the maximum and minimum element sizes, as well as mesh defeaturing. Additionally, local mesh control was implemented at the contact surface between the stationary and rotational domains to ensure that the flow of the working fluid is accurate. The statistics and characteristics of the mesh are specified in Table 4. The cross-sectional view of the generated mesh and overall model can be seen in Figures 19 and 20.

Table 4. Mesh statistics and characteristics.

Property	Value
Default Element Size	50 mm
Growth Rate	1.2
Maximum Size	50 mm
Curvature Minimum Size	0.5 mm
Curvature Normal Angle	18°
Maximum Skewness	0.870
Minimum Orthogonal Quality	0.129
Number of Nodes	3,455,166
Number of Elements	18,672,375

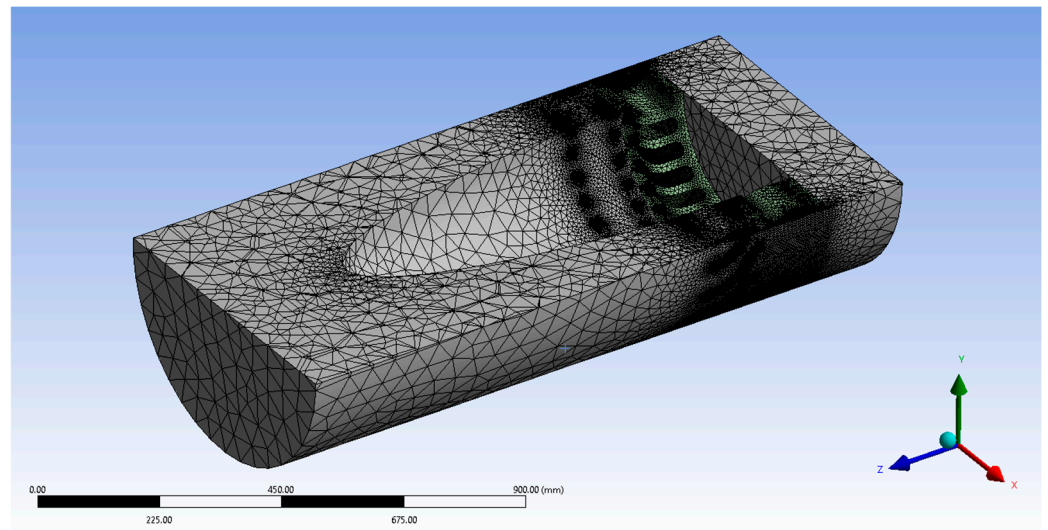


Figure 19. Cross-sectional view of the generated mesh.

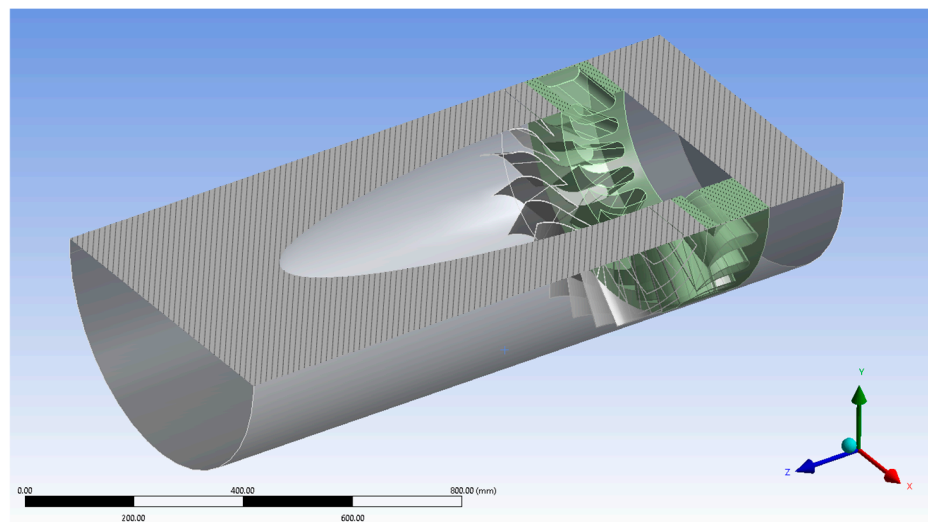


Figure 20. Cross-sectional view of turbine system set-up for CFD simulation.

After successful meshing, the set-up of the simulation was conducted. Firstly, a viscous model for the working fluid was selected. The 2 main choices for this model were k-epsilon and k-omega. According to the Ansys Fluent guides, the k-omega model is considered to perform better near walls, whereas k-epsilon is best suited for flow away from the wall, e.g., free-surface-flow regions [23,24]. As the model has both of those phenomena, the initial simulations were tested with two different models. However, no change in the output values was observed. Therefore, the chosen model was a realisable k-epsilon model with enhanced wall treatment. This is the improved version of a standard k-epsilon model, which was created to close the gap between the standard versions of the 2 models [24]. The previously mentioned moving mesh (also called dynamic mesh) feature was applied to the model to account for the changes in boundary conditions over time in the simulation. This approach is especially important in the fluid–structure interactions of rotating machinery. It promotes the capture of geometry changes within the model, provides better boundary layer resolution, and conserves fluid flow characteristics within the model through accurate tracking of moving boundaries [25].

The standard Ansys water properties were applied to the stationary and rotating domains. The rotating domain was specified as a moving mesh, in order to account for the moving walls of the turbine. The turbine itself was initially set to run at 30 rpm, which was later changed to 130 rpm upon obtaining further results of the 3D fluid behaviour under

operation. The fluid velocity at the inlet was set to 4 m/s, simulating the output of the pumping chamber of the Dolphin device. As the simulation was transient, the operational time was set to 3 s, which accounts for 300 time steps (increments) of 0.01 s size. This was performed to reduce the solution time, as well as the generated sizes of stored files. The overall length of the simulations was validated by referencing the scaled residual graph for the continuity of the simulation, which achieved a stable state. Moreover, the simulation was further examined by comparing the results with 5 and 10 s simulations, which showed a good convergence, with the results for 5 and 10 s being less suitable due to the increased time step size. The set-up simulation was then checked using Ansys Fluent features and solved.

To analyse and validate the results obtained from computational simulations, a previous study dealing with experimental and computational analyses of impulse turbines was considered [22]. This allowed for the identification of suitable measurement points, as well as the values needed to evaluate the turbine’s performance. A total of 4 measurement points were created, which are shown, and colour-coded, in Figure 21.

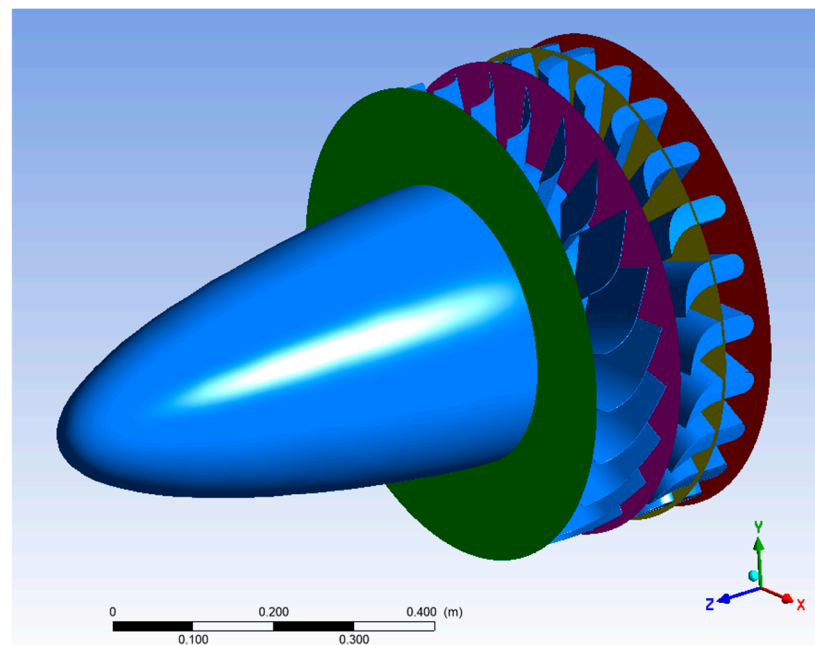


Figure 21. CFD post-measurement locations.

- Position 0—Green—measurement point before the guide vanes, located 200 mm from the midspan of the turbine.
- Position 1—Purple—measurement point after the guide vanes and before the turbine, located 70 mm from the midspan of the turbine.
- Midspan Point—Yellow—measurement point located directly at the midspan of the turbine.
- Position 2—Red—measurement point after the turbine, located –70 mm from the midspan of the turbine.

The evaluation of the turbine’s performance involved the use of the following equations for torque, input power, and flow coefficients, as well as efficiency and power [26]:

$$C_T = T / [p(V_a^2 + U_R^2) b l_r z r_R / 2] \tag{1}$$

$$C_a = \delta_p Q / [p(V_a^2 + U_R^2) b l_r z V_a / 2] \tag{2}$$

$$\varphi = V_a / U_R \tag{3}$$

$$\eta = T\omega / (\delta_p Q) = C_T / (C_a \varphi) \tag{4}$$

$$P = T\omega \tag{5}$$

The overall list of variables and their descriptions can be found in Table 5.

Table 5. List of variables.

Property	Symbol
Torque Coefficient	C_T
Torque	T
Density of Working Fluid	ρ
Axial Flow Velocity	V_a
Circumferential Velocity at r_R	U_r
Height of Blade	b
Chord Length of Rotor Blade	l_r
Number of Rotor Blades	z
Midspan Radius	r_R
Input Power Coefficient	C_a
Total Pressure Drop Across Rotor	δ_p
Flow Rate	Q
Angular Velocity	ω
Flow Coefficient	φ
Efficiency	η
Power	P

As the last step for the CFD analysis of the system, a comparative validation study was conducted. In this study, the developed simulation environment was tested against the previously referenced literature on numerical and experimental testing of the air impulse turbine in OWC [22]. Two main differences can be identified between the referenced study [22] and the investigation conducted in this paper. Firstly, the working fluid in the Dolphin device is water, whereas the OWC turbine is propelled by air. This enforced a change in the domain fluid within the simulations for validation purposes. Secondly, it is crucial to highlight that the system geometries were edited through the previously carried out optimisation techniques for the Dolphin device turbine system. The main differences between the two systems can be seen in Figures 22 and 23.

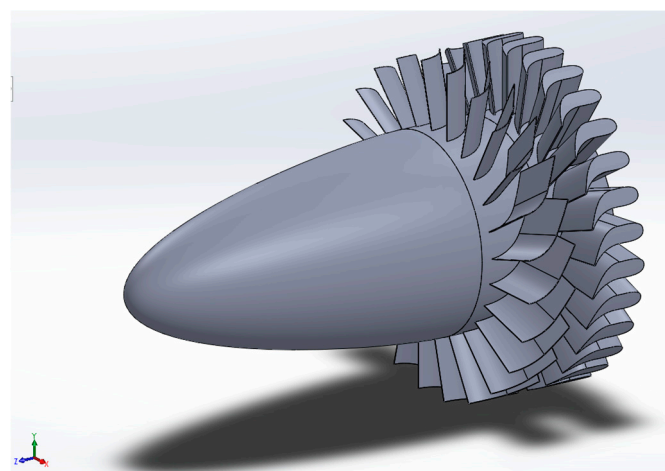


Figure 22. Dolphin device 0.6 m impulse turbine.

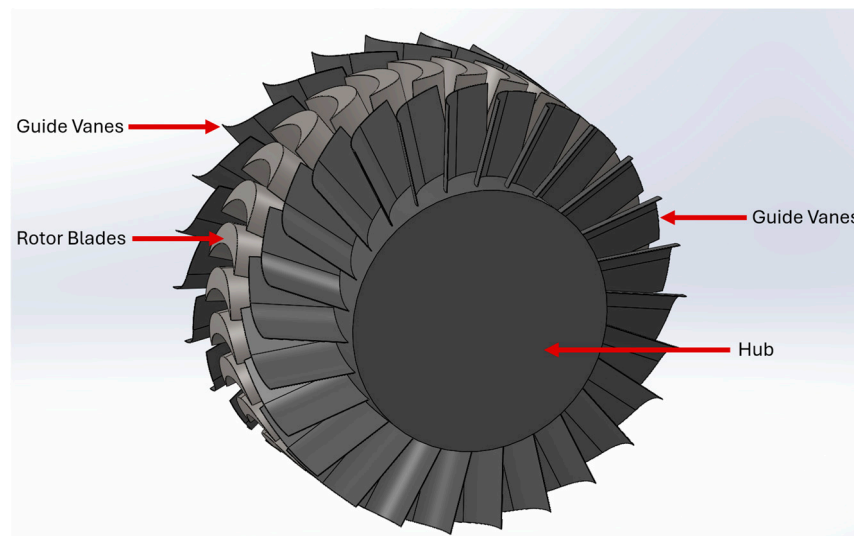


Figure 23. OWC 0.6 m air impulse turbine.

The purpose of this investigation was to validate the overall set-up of the CFD simulations and the behaviour of the fluid throughout the system by comparing the results for the flow coefficient. This meant that the overall axial and circumferential velocities of the fluid at the turbine had to be measured.

The referenced study states that for rotational speeds of the turbine ranging from 125 rpm to 1250 rpm, the recorded flow coefficient ranged from 0.27 to 2.7. Due to the long computational times, the studies for the Dolphin device turbine were limited to the range of 750–1250 rpm, hence a total of 3 simulations with rpm increments of 250 rpm. The required velocities were measured at the midspan of the turbine. Overall, the results showed a good correlation and fit within the specified range, with the flow coefficient ranging from 0.31 to 1.21 for rotational speeds of 1250 rpm to 750 rpm, respectively. Marginal errors are acceptable in both CFD and FEA simulations. Various sources report different error margins, typically ranging from 5% to 13%, depending on the methodology used in the study [27]. Therefore, it was determined that with extensive and complicated CFD simulations with a moving mesh and altered blade geometry, this value difference of 12.9% is acceptable.

2.5. Turbine Design for Manufacturing

The initial model of the turbine was created for the purposes of computational fluid dynamics simulations. Therefore, some features of the turbine could be questioned and deemed not optimal for manufacturing purposes. This required creation of additional concept models, fit for the application. Recognising this situation, further studies on manufacturing adaptability were performed. The turbine's design for manufacturing was conducted after performing CFD simulations. This approach allows the possibility of taking into account the fluid behaviour and the ability to gain more comprehensive knowledge of the operational cycle of the system.

The primary objective of conceptual design is to identify and select the most promising and desirable concepts. The chosen concept is subsequently refined in the design phase. Designers who use efficient and effective concept selection methods are likely to achieve reduced cycle time and costs during the conceptual design stage. Moreover, they can lower the risk of expensive design changes later in the process [28].

A total of 4 different concepts for the turbine were produced. The overall models are presented in Figures 24–27. The permanently fixed blade concept is very similar to the initial design of the turbine, apart from the edited rotor structure and retainment system for the shaft, as well as the specification of permanent fixture—welding. Bolted blades v1 incorporate an off-centre rotor with a retainment system for the blades at the midspan of the rotor. The bolts retaining the blades go through the rotor into the blades; each blade

is given a singular bolt. The bolted blades v2 concept presents a symmetric rotor, along with 2 bolts retaining each of the blades. The slot-in blade turbine consists of blades with a root and 2 rotor plates. The blades slide into a slot on one side of the rotor and are secured by connecting a second rotor plate with bolts. Moreover, the blades are further kept in position by bolts through the root of the blades.

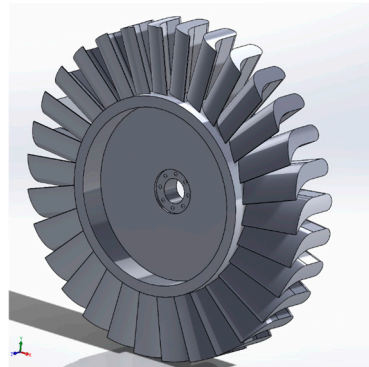


Figure 24. Permanently fixed blades.



Figure 25. Bolted blades v1.



Figure 26. Bolted blades v2.

For easier representation of the general principle of the slot-in turbine, an additional figure was included showing the geometry of the slot-in blade (Figure 28).

The concepts were then appraised according to the specified criteria. Ideally, the chosen design would be simple and easy to manufacture, while maintaining a low cost of development. Moreover, it must provide a satisfactory level of reliability and safety during operation. Lastly, it should be easy to perform maintenance activities on the turbine.

The use of a decision matrix supported the accurate rating completion for the studied concepts against the initial design. An example of such a matrix can be seen in Table 6.



Figure 27. Slot-in blades.

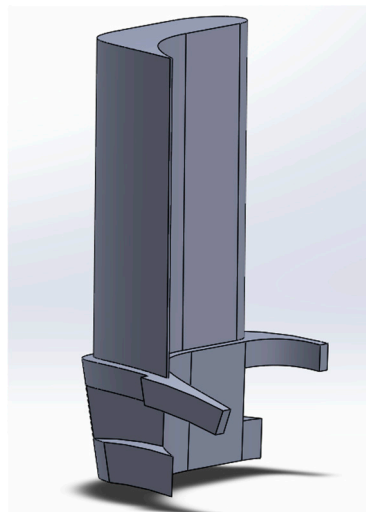


Figure 28. Slot-in blade design concept.

Table 6. Decision matrix.

Concept	Permanently Fixed	Bolted v1	Bolted v2	Slot-In
Manufacturing	-	S	S	-
Development Cost	S	S	S	S
Simplicity	S	S	S	-
Reliability	S	S	S	+
Maintenance	-	+	+	+
Safety	-	S	+	+
+	0	1	2	3
S	3	5	4	1
-	3	0	0	2

Here, “-” is worse, “S” is the same as before, and “+” is improved.

In the case of the manufacturing characteristics, the authors had to appraise the availability of manufacturing capabilities within the project, as well as the suitability of the considered materials. Upon referencing similar studies on 0.6 m impulse turbines for OWC, two suitable materials were selected—aluminium and stainless steel [28]. Aluminium offers a cheaper price per unit volume; however, stainless steel is more commonly used for marine environments, where aggressive corrosion risks are present [29]. When considering this, stainless steel was chosen as a base material for the turbine structure. At the moment of the conducted research, various manufacturing processes were available, such as laser cutting and 5- and 3-axis CNC machining, as well as lathe, milling, and welding machines. This step

became crucial, as some of the complex geometries, e.g., the slot-in blade, would prove to be challenging to manufacture. This issue could be resolved by taking into consideration a significant investment in additive manufacturing. However, this would ultimately increase the overall development and production costs. This is mainly due to the higher operating and material costs.

The permanently fixed blade concept proved to be hard to manufacture due to possible problems with blade alignment while welding. Moreover, the possibility of warped material during welding was also a deciding factor for the negative rating. Due to the permanent fixture, the blades are not easily replaceable, which means that the safety as well as maintenance factors were given a negative rating. When compared to the initial design, the concept was rated to be around the same in terms of development cost, simplicity, and reliability.

The first iteration of the turbine with bolted blades proved to be an improvement in comparison to the permanently fixed turbine set-up. The main quality favouring this solution was the implementation of the detachable blades. This would, overall, reduce the manufacturing complexity and simplify the maintenance of the turbine. There were no expected major changes regarding the development cost and reliability of the system. The second iteration of the bolted blade solution increased the number of constraining points, therefore improving the overall safety of the turbine through a more secure fixture.

Lastly, the slot-in blade turbine concept was evaluated. This iteration was far more complicated in terms of manufacturing complexity and overall design. However, it presents a sturdy fixture system in both radial and theta directions, while maintaining the favourable quality of detachable blades.

The slot-in and bolted v2 concepts ended up with the highest scores, with the bolted v2 design being more centred around the manufacturing complexity and simplicity of the design. Taking into account the current development stage of the project, manufacturing capabilities, and future plans to conduct physical testing on the turbine system, the bolted v2 solution was chosen.

2.6. Generative Design

Complex topologies are often difficult and time-consuming to obtain by conventional optimisation techniques. New analysis and manufacturing methods can be used in an integrated structural optimisation strategy producing highly efficient and adaptive topologies [30]. Metal additive manufacturing has experienced rapid development in recent years, with new commercial metal additive manufacturing machines and methods becoming more competitive and cost-effective in comparison with conventional CNC processes [31,32]. The utilisation of the latest advances in design and manufacturing techniques offers innovative approaches to high-performance structural optimisation applications over different disciplines, such as aerospace, energy, and automotive industries [33]. These new approaches represent a revolution in developing highly efficient and cost-effective strategies at an early stage of design projects and overall manufacturing process [34,35].

Following the development and choice of the best-fitting concept design for the 0.6 m impulse turbine, a generative design structural optimisation process was conducted based on the study [18].

An integrated structural optimisation strategy with generative design techniques was applied to the blade and rotor structure of the Dolphin energy system using the finite element analysis package of ANSYS Workbench 2022. The mesh analysis was adapted to each of the two structures with specific mesh control applied to the boundary surfaces and maintenance of a hexahedron element mesh. The load and fixed conditions were exported from the previous analysis performed in this study and adapted for each of the two structures of the blade and the rotor. The parameters for the generative design process were set with a limit of 500 iterations and a convergence rate of 0.1%. Based on the knowledge acquired in [18], a design for additive manufacturing constraint of an overhang

angle of 35 degrees was also applied to the generative design process in order to minimise the support structure during production.

Firstly, the loading conditions on the system had to be defined and exported from the existing Ansys Fluent project, where a mapping of the pressure acting upon the blades was assessed as shown in Figure 29. The time points for the loading conditions throughout the simulation were analysed and showed marginal differences. The final time step was chosen as the measurement and reference point.

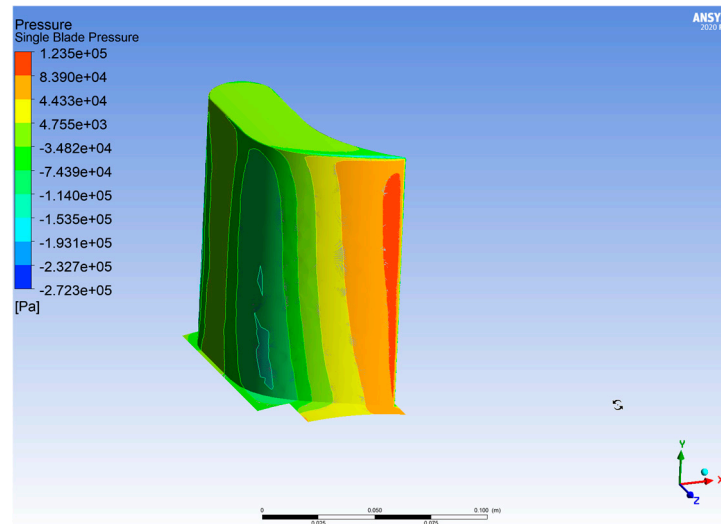


Figure 29. Pressure contour on a turbine blade.

The blade topology was divided into different sectors in order to transfer the pressure acting upon the surface of the blade to develop the generative design structural optimisation. In Figure 30, we can observe the divisions of the surface of the blade into different facets.

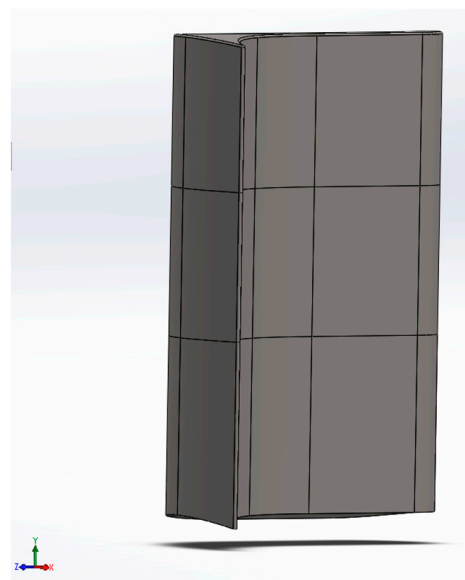


Figure 30. Divided blade surface—facet location.

Using the results obtained from the Ansys Fluent simulation, an average pressure value was calculated for each of the facets conforming to the four surfaces of the blade. In Table 7, the different pressure values associated with each of the facets can be seen.

Table 7. Divided blade surface with facet location and average pressure values.

Blade Surface	Average Pressure over the Facets (Pa)
	P1.1: −22,873.8 P1.2: 72,313.4 P1.3: −45,908 P1.4: 60,797.4 P1.5: −53,121.4 P1.6: 53,477.6
	P2.1: −45,370.8 P2.2: −5974.4 P2.3: −381 P2.4: −40,723.4 P2.5: −27,486.8 P2.6: −7503.4 P2.7: −167,665 P2.8: −29,099.8 P2.9: −9546.4
	P3.1: −47,375.4 P3.2: −17,752.2 P3.3: −20,236.4 P3.4: −94,448.8 P3.5: −16,628.2 P3.6: −75,365
	P4.1: −21,531.6 P4.2: −64,712.4 P4.3: −29,843.8 P4.4: −86,777 P4.5: −30,178.2 P4.6: −92,683

The calculated pressure values were used to develop the boundary conditions of the blade generative design structural optimisation process. In Figure 31, the applied pressures are shown in red and the fixed support representing the bolted joint with the rotor structure is shown in blue.

The nature of the loads acting upon the structure of the blade constrains the outer surface of the topology as a boundary condition, limiting the volume optimisation range of the internal volume. The advantage of a design for an additive manufacturing approach allows for the consideration of hollow cavities as part of the optimisation process. Figure 32 shows the generative design structural optimisation process of the blade representing the initial stage of the process with the considerations of the boundary conditions, a middle stage of the optimisation process where mass is generated to comply with the optimisation objectives, and the final converged solution of the generative design process.

In order to develop the generative design structural optimisation for the rotor topology, a resultant force was calculated to transfer the pressure acting upon the blades into the rotor structure through the bolted joints. We can observe the resultant force calculated in Figure 33.

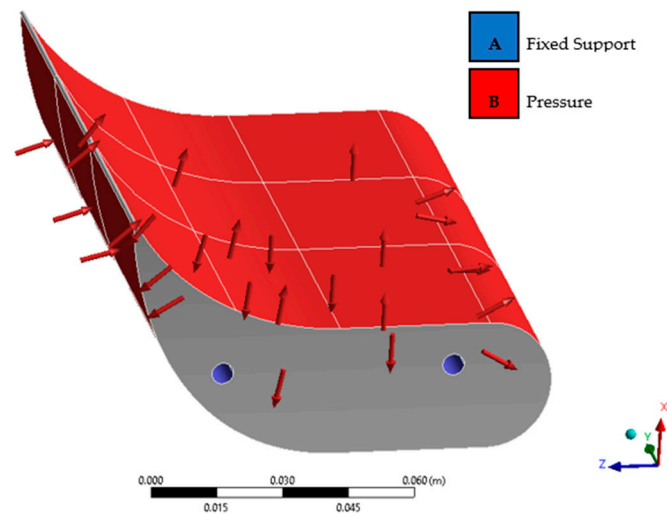


Figure 31. Divided blade surface with transferred pressure over individual facets.

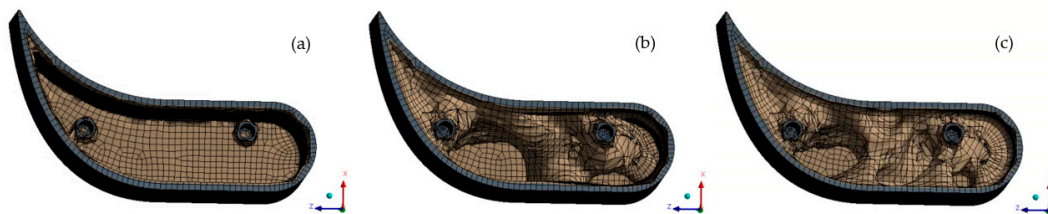


Figure 32. Generative design structural optimisation process of the blade: (a) the initial iteration of the generative design process; (b) the middle stage of the generative design process; (c) the final converged solution of the generative design process.

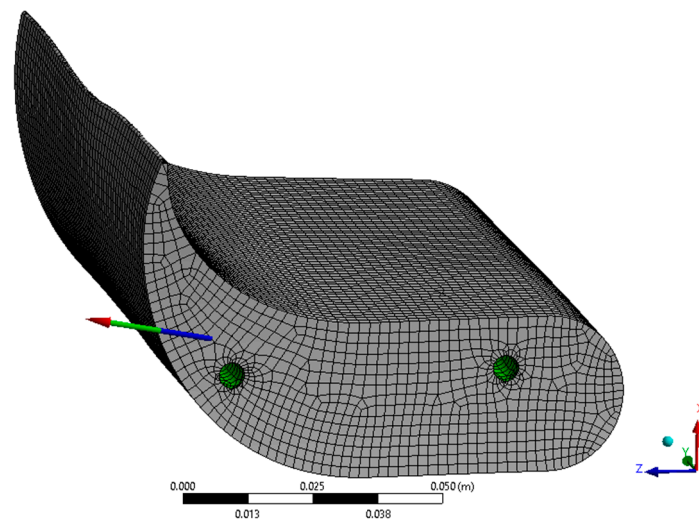


Figure 33. The resultant force generated by the pressure acting upon the blade structure.

Table 8 represents the values of the different components of the resultant force, with a total value of 475.99 N. In this table, we can observe that the value of the component of the resultant force in the y-axis is negligible in comparison with the x and z components of the force.

Table 8. Divided blade surface with facet location and average pressure values.

Force Component	Force Value (N)
X component	87.266
Y component	-3.0223×10^{-3}
Z component	467.92
Total	475.99

Following the assessment of the resultant force generated by the pressure acting upon the blade structure, a load was applied on the rotor structure’s bolted joint surface, as can be seen in Figure 34a marked in red. For an efficient application of the resultant force to each of the 30 blades’ bolted fixed constraints, the component of the force in the z-axis was maintained constant while the x component was translated and rotated for each of the blades’ bolted fixed constraints, as we can observe in Figure 34b. In Figure 34b, the gravitational load applied on the centre of mass, a 13.6 rad/s rotational velocity as a worst-case scenario for the turbine operation, and a fixed constraint for the rotor structure on the bolted connection at the shaft are shown.

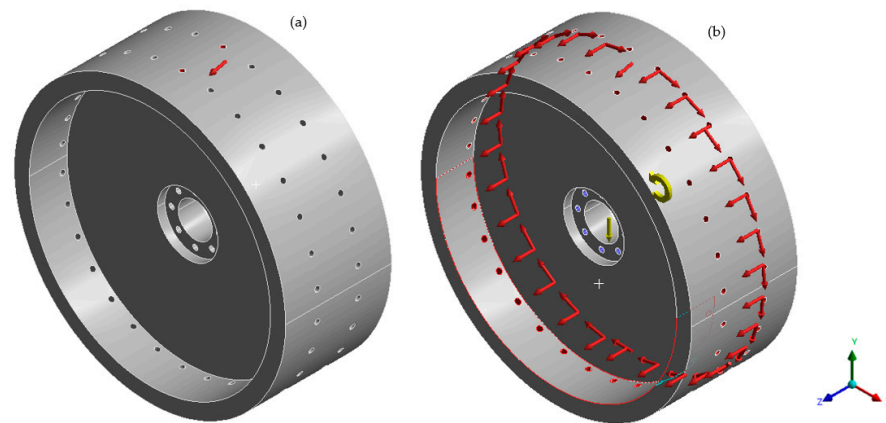


Figure 34. The resultant force generated by the pressure acting upon the blade structure transferred into the rotor structure; (a) the single blade resultant force applied on the blade is bolted fixed constraints; (b) boundary conditions of the rotor structure.

Figure 35 shows the generative design structural optimisation process of the rotor structure including the initial stage of the process with the considerations of the boundary conditions, a middle stage of the optimisation process where mass is generated to comply with the optimisation objectives, an advanced stage of the optimisation process, and the final converged solution of the generative design process.

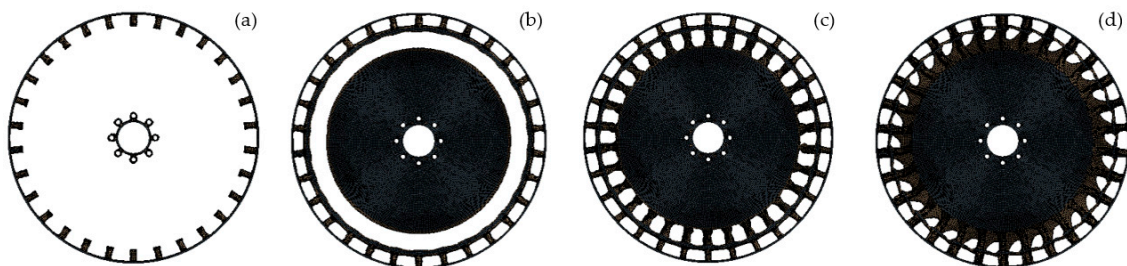


Figure 35. Generative design structural optimisation process of the rotor topology; (a) the initial iteration of the generative design process with boundary conditions; (b) the middle stage of the generative design process; (c) an advanced stage of the generative design process; (d) the final converged solution of the generative design process.

3. Results

The investigations performed in Ansys Fluent resulted in accurate predictions of fluid behaviour under the turbine’s operation, which can be seen in Figure 36.

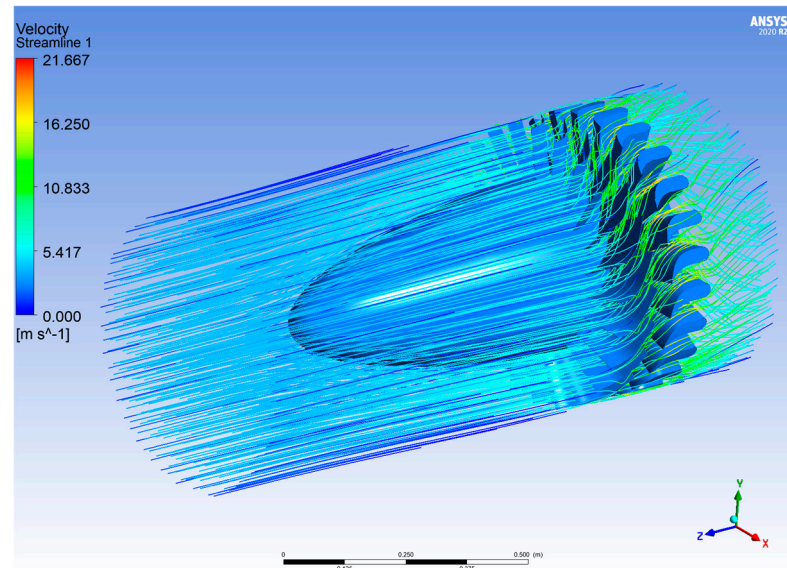


Figure 36. Fluid flow in 3D CFD turbine system simulation.

With the initial fluid velocity of 4 m/s, a substantial increase can be observed at the guide vanes, as well as the turbine area. The maximum velocity reached by the working fluid was 21.67 m/s, thus over five times the initial speed. This result correlates with the prior predictions of 2D simulations. Moreover, the high velocity at the outlet validates the aim of improving the water extraction capabilities and marking the improvement in reference to the initial design of the turbine system.

As mentioned before, the primary aim of the CFD simulations was to evaluate the performance of the current turbine design. With the use of previously described measurement points, necessary variables for the calculation of power, torque, and input power coefficients, as well as efficiency, were obtained. The variable components’ values for an initial fluid velocity of 4 m/s and a turbine rotational speed of 130 rpm can be seen in Table 9.

Table 9. CFD simulation results for considered variables.

Symbol	Variable	Value
T	Torque	1886 [Nm]
ρ	Density of Working Fluid	998.2 [kg/m ³]
V_a	Axial Flow Velocity	8.126 [m/s]
U_R	Circumferential Velocity at r_R	4.08 [m/s]
b	Height of Blade	0.1186 [m]
l_r	Chord Length of Rotor Blade	0.1002 [m]
z	Number of Rotor Blades	30
r_R	Midspan Radius	0.3 [m]
δ_p	Total Pressure Drop Across Rotor	49,436 [Pa]
Q	Flow Rate	0.84 [m ³ /s]
ω	Angular Velocity	130 [rpm]

The flow rate present in the turbine system was calculated by multiplying the axial flow velocity by the total flow area at the turbine midspan equal to 0.103 m². Moreover, the pressure drop across the rotor was calculated by obtaining pressure values at measurement

points Position 1 and Position 2. The final values for power, torque coefficient, input power coefficient, and efficiency are given as follows:

$$C_T = 0.4962 \quad (6)$$

$$C_a = 0.4036 \quad (7)$$

$$\varphi = 3.57 \quad (8)$$

$$\eta = 0.6179 \quad (9)$$

$$P = 25,675.19 \text{ W} \quad (10)$$

Ultimately, the performance of the studied turbine was determined. The power output was estimated to be 25,675.19 W with a turbine efficiency of 61.79%.

Through the use of the decision matrix in the design for manufacturing studies, the most favourable concept was chosen. The bolted v2 turbine concept design (Figure 37) proved to be the best solution for the current stage of the project after taking into account the available resources, such as the manufacturing capabilities.



Figure 37. Selected bolted v2 turbine concept design.

The generative design structural optimisation allowed the exploration of non-conventional topologies and new manufacturing techniques, producing a more efficient and cost-effective design process. In Figure 38, the topologies generated by this process for the blade and rotor structures can be seen.

The use of design for additive manufacturing constraints also allows the optimisation of the generated topology in order to reduce the support material needed for the printing process by adapting the overhang angle limit, which, in this case, is set at 35°. The generative design optimisation minimises the overhang angles of the generated topologies under the established limit. In Figure 39, an example of the implications of the use of design for additive manufacturing constraints can be seen in the section view of the generated rotor structure (b). While an additional support structure is still needed for the bottom flat surface of the disc, the use of an additional support structure is avoided for the internal cavities and angled columns.

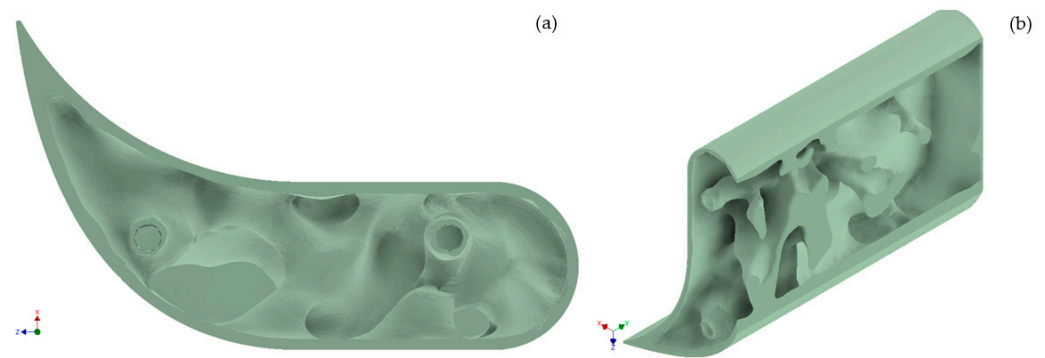


Figure 38. Generative design optimisation results of the blade structure; (a) bottom view of the generated topology of the blade; (b) section view of the generated topology of the blade.

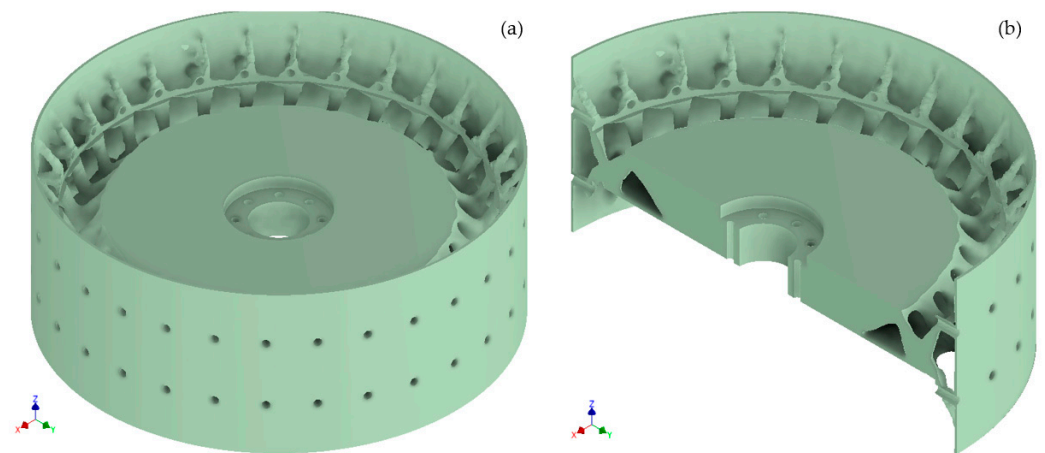


Figure 39. Generative design optimisation results of the rotor structure; (a) isometric view of the generated topology of the rotor; (b) section view of the generated topology of the rotor.

In Table 10, the results for the generative design structural optimisation can be seen, where both structures experience over 60% in weight reduction, 60.226% for the blade and 69.523% for the rotor, with a final mass of 1 kg and 14.4 kg, respectively. A substantial increment in computational time can be obtained for the rotor structure due to a large amount of boundary surfaces and wide optimisation volume ranges, producing a computational time of 14 h and 8 min, in comparison with the 28 min of the blade structure.

Table 10. Generative design structural optimisation results.

	Blade Structure	Rotor Structure
Mesh Analysis	Element size: 0.002 m Method: hexahedrons Nodes: 228,167 Elements: 61,438	Element size: 0.002 m Method: hexahedrons Nodes: 3,991,615 Elements: 1,080,272
Generative Design Optimisation	47 iterations Convergence: 0.1% Time: 28 min 57 s	60 iterations Convergence: 0.1% Time: 14 h 8 min
Initial Mass	2.5205 kg	47.303 kg
Final Mass	1.0025 kg	14.417 kg
Mass Reduction	60.226%	69.523%

Computational Sustainability

Over the course of any R&D project supported by computational calculations, a significant number of simulations will be conducted. Therefore, it is essential to limit

the computational times and improve the overall performance of calculation activities, thus supporting the idea of sustainable modelling and analysis. The solution times for simulations should always be minimised, regardless of available resources and hardware, without compromising the accuracy of the study. Shorter solution times can lead to a more cost-effective, productive, and efficient workflow [36].

By simplifying the turbine system used in this investigation (increase in the tip clearance), the overall computational times were reduced. Moreover, the use of additional features such as local mesh control can help to directly specify the required size of the elements at the area of interest, which can further optimise the solution times.

The total solution times for conducted simulations considered in the computational sustainability study are presented in Table 11.

Table 11. Details of performed simulations regarding computational performance.

Software	Type of Simulation	No. of Simulations	Solution Time (Average)
Ansys 2020	3D Turbine CFD Simulation rev1	2	19 h
Ansys 2020	3D Turbine CFD Simulation rev2	6	10.5 h
Ansys 2020	3D Turbine Meshing	2	15 min
Ansys 2020	3D Turbine Meshing	3	7 min
SolidWorks 2023	3D Turbine CFD Simulation Rev1	3	19 min
SolidWorks 2023	3D Turbine CFD Simulation Rev2	4	13 min
Ansys 2020	Blade Generative Design	1	28 min
Ansys 2020	Rotor Generative Design	1	14 h

The simulation revisions refer to the mentioned optimisation techniques used, with revision 1 simulations being performed before the optimisation. Three-dimensional turbine CFD simulations for revision 1 were substantially longer than revision 2 with resultant improvements of almost 81% for Ansys Fluent simulation and 46% for SolidWorks. This substantial decrease in solution times can validate the importance of computational sustainability studies and promote the gathering of data for future investigations.

It is also important to make note of the specifications of the computer system used, which are given in Table 12.

Table 12. Computer specifications.

Property	Specification
GPU	NVIDIA GeForce RTX 4070
CPU	Intel® Core™ I7—14700KF
RAM	32 GB
Disc	SSD

4. Discussion

Through the conducted investigations, the application of a 0.6 m impulse turbine in a Dolphin wave energy conversion device was appraised. The initial 2D CFD simulations evaluated the overall system response and fluid behaviour. Moreover, using parametric optimisation, an optimal geometry for the guide vanes and turbine blades was found. This led to the development of a 3D turbine model for CFD simulation application. During those studies, the interaction between the power generation unit and the working fluid could be further examined and specified. Through the use of measurement points, the necessary characteristics of the turbine were obtained. They were later incorporated into referenced power, torque, and power input coefficients, as well as efficiency formulas. This

ultimately resulted in an evaluation of the performance of the turbine and validated the use of the impulse turbine design for the Dolphin wave energy conversion device.

The design for manufacture investigation incorporated the development of potential concept designs for the Dolphin device turbine system. A total of four concepts were presented in this study and appraised using a decision matrix. The matrix consisted of six characteristics: manufacturing, development cost, simplicity, reliability, maintenance, and safety. The two concepts with the highest scores—bolted v2 and slot-in—were taken into consideration. Ultimately, the chosen concept for further studies was bolted v2. This was due to available manufacturing capabilities and future plans related to the physical testing of the turbine system in a physical setting.

The promising capabilities of implementing the latest design and manufacturing techniques as an integrated structural optimisation strategy represent a revolution in sustainable design processes. The combination of generative design and metal additive manufacturing opens the door to more efficient and adaptative results [33]. The flexibility of the optimisation process while integrating the relevant design parameters into the process generates fit-for-purpose topologies specific to each application as previously demonstrated in [18]. A full understanding of the parameters of metal additive manufacturing as an integrated part of optimisation processes will enhance the efficiency and sustainability of structural design techniques [33].

The study on computational sustainability showed a great improvement upon revision of the 3D turbine model and application of additional features controlling the size of the generated mesh. Overall, the model optimisation resulted in shorter solution times ranging from 46% to 81% reductions. Thus, the significance of computational sustainability was established, promoting the gathering of data for future investigations.

5. Conclusions

The carried-out investigation on the 0.6 m impulse turbine resulted in the identification of this innovative methodology for the structural optimisation of the mentioned new wave energy device through the use of CFD and FEA simulations, parametric optimisation on the blade structure, a generative design optimisation for the blade and rotor structures integrating the results of the CFD and FEA simulations as inputs, and a design for an additive manufacturing approach. The conducted studies showed an efficiency of 61.79% and power generation capabilities of 25,675.19 W. Moreover, through the generative design optimisation, the overall masses of the blade and rotor structure were reduced by 60.226% and 69.523%, respectively.

The overall process consisted of the identification of a suitable solution for the turbine system working in an offshore environment under specified conditions. The system was then initially analysed through 2D CFD simulation with incorporated parametric optimisation. Subsequently, the optimised components were modelled in 3D and investigated in transient CFD simulation. The set-up of the 3D CFD simulation was then validated through the referenced literature. A satisfactory level of flow coefficient convergence was observed between the two studies.

The generative design optimisation process consisted of exporting the loads, and fixture conditions from the previous CFD studies were evaluated on the developed 3D model. The process was further broken down into two stages, where the blade structure and rotor structure were analysed separately. The generative design optimisation promoted the idea of exploring unconventional design topologies and showed the potential of additive manufacturing in design automation.

Further research directions include developing CAM models for CNC manufacturing, aiming to produce the turbine system for physical testing in a water tank. While this study's computational analysis was carefully checked against published data to confirm its reliability, additional experimental testing would be valuable to further support the findings. By carrying out these physical tests, the results from this paper could be con-

firmed in real-world conditions, adding another layer of validation to already existing investigation conclusions.

Author Contributions: Conceptualisation, S.S. and P.J.-S.; methodology, S.S., P.J.-S. and D.G.D.; software, S.S. and D.G.D.; validation, S.S.; formal analysis, S.S. and D.G.D.; investigation, S.S. and D.G.D.; resources, S.S. and D.G.D.; data curation S.S., P.J.-S. and D.G.D.; writing—original draft preparation, S.S. and D.G.D.; writing—review and editing, P.J.-S. and E.O.; visualisation, S.S. and D.G.D.; supervision, P.J.-S. and E.O.; project administration, P.J.-S.; funding acquisition, P.J.-S. All authors have read and agreed to the published version of the manuscript.

Funding: Energy Technology Partnership [ETP] in collaboration with Edinburgh Napier University and Pentland Materials Supply Ltd., through ETP Energy Industry Doctorate Programme, reference number ETP PhD #227.

Institutional Review Board Statement: Not applicable.

Informed Consent Statement: Not applicable.

Data Availability Statement: Data are contained within the article.

Acknowledgments: The authors would like to acknowledge the contribution of Pentland Materials Supply Ltd., in particular, John Lock and Robert McCartney, for their contribution to the development of this project.

Conflicts of Interest: The authors declare no conflicts of interest.

References

- Doleh, Z.K.; Lock, J. Shutter Valve and Device for Generating Energy from Sea Waves Comprising Such. Valves. Patent US10145353B2, 2 June 2015.
- Thorpe, T. An Overview of Wave Energy Technologies: Status, Performance and Costs. *Wave Power Mov. Towards Commer. Viability* **1999**, *26*, 50–120.
- Cashman, A.P. Design and Optimisation of the Impulse Turbine with an Internal Variable-Pitch Controlled Guide Vane System Using Computational Fluid Dynamics and Experimental Analysis, A. University of Limerick, 2012. Available online: <https://hdl.handle.net/10344/5816> (accessed on 21 July 2024).
- O'Brien, L.; Christodoulides, P.; Renzi, E.; Stefanakis, T.; Dias, F. Will oscillating wave surge converters survive tsunamis? *Theor. Appl. Mech. Lett.* **2015**, *5*, 160–166. [CrossRef]
- Kofoed, J.P.; Frigaard, P.; Friis-Madsen, E.; Sørensen, H.C. Prototype testing of the wave energy converter wave dragon. *Renew. Energy* **2006**, *31*, 181–189. [CrossRef]
- Friss-Madsen, E. Feasibility and LCA for Wave Dragon, Economics of Offshore Wave Energy, ISOPE Presentation. Available online: <https://www.wavedragon.com/> (accessed on 19 November 2024).
- Energy and Climate Change Directorate, Scottish Government Climate Change Plan. Available online: <https://www.gov.scot/policies/climate-change/> (accessed on 21 July 2024).
- Wave Energy Scotland. Policy and Innovation Group: UK Ocean Energy Review. Available online: <https://www.waveenergyscotland.co.uk/news-events/2023-uk-ocean-energy-review-report-published/> (accessed on 21 July 2024).
- Scottish Energy and Climate Change Directorate. Energy Strategy: Position Statement. Available online: <https://www.gov.scot/publications/scotlands-energy-strategy-position-statement> (accessed on 21 July 2024).
- Ocean Energy Europe. Ocean Energy: Key Trends and Statistics. March 2023. Available online: <https://www.oceanenergy-europe.eu/wp-content/uploads/2023/03/Ocean-Energy-Key-Trends-and-Statistics-2022.pdf> (accessed on 21 July 2024).
- Guo, B.; Ringwood, V. A review of wave energy technology from a research and commercial perspective. *IET Renew. Power Gener.* **2021**, *15*, 3065–3090. [CrossRef]
- Masterson, V. Wave Energy: Can Ocean Power Solve the Global Energy Crisis? Available online: <https://www.weforum.org/agenda/2022/03/wave-energy-ocean-electricity-renewables/> (accessed on 21 July 2024).
- Diesing, P.; Bogdanov, D.; Satymov, R.; Child, M.; Hauer, I.; Breyer, C. Offshore versus onshore: The underestimated impact of onshore wind and solar photovoltaics for the energy transition of the British Isles. *Renew. Power Gener.* **2023**, *17*, 3240–3266. [CrossRef]
- Clean Power. A Window into the Future of Wave Energy. Available online: <https://cleantechnica.com/2022/02/18/a-window-into-the-future-of-wave-energy/amp/> (accessed on 21 July 2024).
- Mapitsis, A.; Kapasakalis, K.; Via-Estrem, L. An integrated FEA-CFD simulation of offshore wind turbines with vibration control systems. *Eng. Struct.* **2022**, *254*, 113859.
- Jaen-Sola, P.; McDonald, A.S.; Oterkus, E. *A Lightweight Approach for Airborne Wind Turbine Drivetrains*; European Wind Energy Association: Brussels, Belgium, 2015; pp. 1–9.

17. Pastor, J.; Liu, Y. Power Absorption Modeling and Optimization of a Point Absorbing Wave Energy Converter Using Numerical Method. *J. Energy Resour. Technol.* **2014**, *136*, 021207. [[CrossRef](#)]
18. Gonzalez-Delgado, D.; Jaen-Sola, P.; Oterkus, E. A New Zero Waste Design for a Manufacturing Approach for Direct-Drive Wind Turbine Electrical Generator Structural Components. *Machines* **2024**, *12*, 643. [[CrossRef](#)]
19. Jack, A. *Initial CFD Analysis of a Flooded Turbine in a Wave Pump Generator*; Edinburgh Napier University: Edinburgh, UK, 2022.
20. Thandayutham, K.; Samad, A.; Badhurshah, R. Performance Enhancement of an Impulse Turbine Used for Ocean Energy Extraction. In Proceedings of the 5th International Congress on Computational Mechanics and Simulation, Chennai, India, 10–13 December 2014. [[CrossRef](#)]
21. Setoguchi, T.; Kaneko, K.; Maeda, H.; Kim, T.W.; Inoue, M. Impulse Turbine with Self-Pitch-Controlled Guide Vanes for Wave Power Conversion: Performance of Mono-Vane Type. *Int. J. Offshore Polar Eng.* **1993**, *3*, 73–78.
22. Thakker, A.; Dhanasekaran, T.S. Experimental and computational analysis on guide vane losses of impulse turbine for wave energy conversion. *Renew. Energy* **2005**, *30*, 1359–1372. [[CrossRef](#)]
23. Ansys Fluent, Chapter 4: Turbulence, Release 2020 R2. In *Ansys Fluent Theory Guide*; Ansys, Inc.: Canonsburg, PA, USA, 2020.
24. Ansys Fluent, Chapter 13: Modelling Turbulence, Release 2020 R2. In *Ansys Fluent User's Guide*; Ansys, Inc.: Canonsburg, PA, USA, 2020.
25. Doustdar, M.M.; Kazemi, H. Effects of a fixed and dynamic mesh methods on simulation of stepped planing craft. *J. Ocean. Eng. Sci.* **2019**, *4*, 33–48. [[CrossRef](#)]
26. Setoguchi, T.; Santhakumar, S.; Maeda, H.; Takao, M.; Kaneko, K. A review of impulse turbines for wave energy conversion. *Renew. Energy* **2001**, *23*, 261–292. [[CrossRef](#)]
27. Rahman, H.A. Finite Element Model Updating of Dissimilar Plate with Rivet Joint. *IOP J. Phys. Conf. Ser.* **2019**, *1262*, 012035. [[CrossRef](#)]
28. Thakker, A.; Jarvis, J.; Buggy, M.; Sahed, A. 3DCAD conceptual design of the next-generation impulse turbine using the Pugh decision-matrix. *Mater. Des.* **2009**, *30*, 2676–2684. [[CrossRef](#)]
29. Istrate, G.G.; Muresan, A.C. *Corrosion Behaviour of Materials Al5083 Alloy, 316L Stainless Steel and A681 Carbon Steel in Seawater*; University of Galați: Galați, Romania, 2021. [[CrossRef](#)]
30. Zhu, J.; Zhou, H.; Wang, C.; Zhou, L.; Yuan, S.; Zhang, W. A review of topology optimization for additive manufacturing: Status and challenges. *Chin. J. Aeronaut.* **2021**, *34*, 91–110. [[CrossRef](#)]
31. Ali, M.H.; Sabyrov, N.; Shehab, E. Powder bed fusion–laser melting (PBF–LM) process: Latest review of materials, process parameter optimization, application, and up to date innovative technologies. *Addit. Manuf.* **2022**, *7*, 1395–1422. [[CrossRef](#)]
32. Nyamekye, P.; Unt, A.; Salminen, A.; Piili, H. Integration of Simulation Driven DFAM and LCC Analysis for Decision Making in L-PBF. *Metals* **2020**, *10*, 1179. [[CrossRef](#)]
33. Blakey-Milner, B.; Gradl, P.; Snedden, G.; Brooks, M.; Pitot, J.; Lopez, E.; Leary, M.; Berto, F.; du Plessis, A. Metal additive manufacturing in aerospace: A review. *Mater. Des.* **2021**, *209*, 110008. [[CrossRef](#)]
34. Sæterbø, M.; Solvang, W.D. Evaluating the cost competitiveness of metal additive manufacturing—A case study with metal material extrusion. *CIRP J. Manuf. Sci. Technol.* **2023**, *45*, 113–124. [[CrossRef](#)]
35. Monteiro, H.; Carmona-Aparicio, G.; Lei, I.; Despeisse, M. Energy and material efficiency strategies enabled by metal additive manufacturing—A review for the aeronautic and aerospace sectors. *Energy Rep.* **2022**, *8*, 298–305. [[CrossRef](#)]
36. Szatkowski, S.; Jaen-Sola, P.; Oterkus, E. An Efficient Computational Analysis and Modelling of Transferred Aerodynamic Loading on Direct-Drive System of 5 MW Wind Turbine and Results Driven Optimisation for a Sustainable Generator Structure. *Sustainability* **2024**, *16*, 545. [[CrossRef](#)]

Disclaimer/Publisher's Note: The statements, opinions and data contained in all publications are solely those of the individual author(s) and contributor(s) and not of MDPI and/or the editor(s). MDPI and/or the editor(s) disclaim responsibility for any injury to people or property resulting from any ideas, methods, instructions or products referred to in the content.